Vascular Endothelial Growth Factor (VEGF)-A165b Is a Weak *In vitro* Agonist for VEGF Receptor-2 Due to Lack of Coreceptor Binding and Deficient Regulation of Kinase Activity

Harukiyo Kawamura,[1] Xiujuan Li,[1] Steven J. Harper,[2] David O. Bates,[2] and Lena Claesson-Welsh[1]

[1]Department of Genetics and Pathology, Rudbeck Laboratory, Uppsala University, Uppsala, Sweden; and [2]Microvascular Research Laboratories, Bristol Heart Institute, Department of Physiology and Pharmacology, School of Veterinary Sciences, University of Bristol, Bristol, United Kingdom

Abstract

Vascular endothelial growth factor (VEGF)-A165b is a COOH-terminal splice variant of VEGF-A that has been implicated in negative regulation of angiogenesis. We compared the properties of VEGF-A165b with those of VEGF-A121, VEGF-A145, and VEGF-A165. Induction of tyrosine phosphorylation sites in VEGFR-2 differed between the VEGF ligands as determined by tryptic phosphopeptide mapping and by use of phosphosite-specific antibodies. VEGF-A165b was considerably poorer in inducing phosphorylation of the positive regulatory site Y1052 in VEGFR-2. Whereas this did not affect activation of VEGFR-2 *in vitro*, we show that VEGF-A165b failed to induce vasculogenesis and sprouting angiogenesis in differentiating embryonic stem cells and vascularization of s.c. Matrigel plugs. In addition, the ability of the different VEGF ligands to induce angiogenesis correlated with their abilities to bind the VEGF coreceptor neuropilin 1 (NRP1). Our data indicate that loss of VEGFR-2/NRP1 complex formation and Y1052 phosphorylation contribute to the lack of angiogenic properties of VEGF-A165b. [Cancer Res 2008; 68(12):4683–92]

Introduction

Vascular endothelial growth factor (VEGF)-A is a potent regulator of physiologic and pathologic angiogenesis (1). VEGF belongs to the cysteine-knot family of growth factors, which also includes platelet-derived growth factors and stem cell factor. Structurally, VEGF-A is composed of two identical polypeptide chains oriented in an antiparallel manner (2). The *vegf-a* gene encompasses eight exons that are alternatively spliced to create isoforms designated according to their number of amino acid residues (such as VEGF-A121, VEGF-A145, and VEGF-A165; ref. 3). VEGF-A165b is an endogenous COOH-terminal splice variant identified in 2002 (4). VEGF-A165 and VEGF-A165b are structurally identical except for the unique COOH-terminal sequence of six amino acid residues, CDKPRR in VEGF-A165 compared with SLTRKD in VEGF-A165b, encoded by alternative exons 8a and 8b.

The VEGF-A isoforms bind with high affinity to two related receptor tyrosine kinases denoted VEGF receptor (VEGFR)-1 and VEGFR-2 (5). VEGFR-1 is expressed on circulating hematopoietic cells as well as on endothelial cells, whereas VEGFR-2 is expressed on circulating endothelial precursors and on mature endothelial cells. Inactivation of a single *vegf-a* allele in mice results in early lethality at embryonic day (E)11-12 due to deficient endothelial cell development and lack of vessels (6, 7). *Vegfr-2*$^{-/-}$ animals die at E8.5 with a phenotype similar to that of *vegf-a*$^{-/-}$ animals (8). VEGFR-2 is therefore regarded as a main transducer of VEGF biology in vasculogenesis and angiogenesis (5).

In addition to VEGFR-1 and VEGFR-2, endothelial cells express VEGF coreceptors, neuropilin 1 (NRP1) and heparan sulfate proteoglycan (HSPG), which interact with the VEGF-A isoforms to different extents. HSPGs bind to VEGF-A through exons 6 and 7, and NRP1 through exon 7 (see ref. 9 for a review). Exon 8 has also been implicated in NRP1 binding (10). HSPGs are transmembrane, glycosylphosphatidylinositol-anchored, or secreted proteins with covalently linked HS chains, which stabilize the ligand/receptor complex and thereby modulate the activity of secreted growth factors (11). Expression of HS on endothelial cells is critical for VEGF responsiveness (12). We have previously described that presentation of VEGF-A by HS expressed by an adjacent cell, rather than by the endothelial cell itself, leads to prolonged half-life of the VEGFR-2 signaling complex (13). NRP1 is a transmembrane glycoprotein with a short cytoplasmic domain that lacks intrinsic catalytic activity. NRP1 was first identified as a receptor for class 3 semaphorins, a family of soluble molecules engaged in neuronal guidance (14, 15), and subsequently, NRP1 was found to bind VEGF-A as well (16). Targeted inactivation of the mouse *nrp1* gene leads to severe defects in both neuronal and vascular development and embryonic lethality around E12.5 (17).

VEGF-A165b has been reported to bind VEGFR-2 with the same affinity as VEGF-A165, but still, it lacks angiogenic properties. Moreover, through as yet unknown mechanisms, VEGF-A165b blocks the ability of VEGF-A165 to induce angiogenesis. Several *in vivo* responses to VEGF-A165 are blocked by VEGF-A165b, such as vascularization in the rabbit cornea, the rat mesentery, the chicken embryo chorioallantoic membrane, and xenotransplanted cancer cells in mice (4, 18, 19–21). In the present study, we have determined the mechanism of loss of function of VEGF-A165b. For this purpose, we have compared its effect with that of other VEGF isoforms with regard to its ability to engage VEGF coreceptors, to induce vessel formation *in vitro* and *in vivo*, and to induce various VEGFR-2 tyrosine phosphorylation sites. We find many similarities between VEGF-A121 and VEGF-A165b; both lack NRP1-binding ability and fail to induce endothelial cell organization into vessel structures in embryoid bodies (EB) and in s.c. Matrigel plugs. An important distinctive feature of VEGF-A165b is its markedly

Note: Current address for H. Kawamura: Department of Clinical Cell Biology, Chiba University Graduate School of Medicine, 1-8-1 Inohana, Chuo-ku, Chiba 260-8670, Japan.

Requests for reprints: Lena Claesson-Welsh, Department of Genetics and Pathology, Rudbeck Laboratory, Uppsala University, Dag Hammarskjöldsv. 20, 751 85 Uppsala, Sweden. Phone: 46-184714363; Fax: 46-18558931; E-mail: Lena.Welsh@genpat.uu.se.

doi:10.1158/0008-5472.CAN-07-6577

reduced ability to induce phosphorylation of positive regulatory tyrosine residues in VEGFR-2.

Materials and Methods

Antibodies and growth factors. The following antibodies were used: anti-NRP1 (C-19; Santa Cruz Biotechnology), anti-human VEGFR-2 (R&D Systems), anti-phosphorylated VEGFR-2/3 (against phosphorylated Y1054/Y1059; Merck), phosphorylated VEGFR-2 rabbit monoclonal antibody (mAb; against phosphorylated Y1175; 19A10; Cell Signaling Technology), and phosphorylated VEGFR-2 rabbit mAb (against phosphorylated Y1212; 11A3; Cell Signaling Technology). IRDye 800–conjugated affinity-purified anti-goat IgG (Rockland Immunochemicals), mouse monoclonal anti-phosphotyrosine 4G10 (Upstate Biotechnology), enhanced chemiluminescence (ECL) anti-rabbit IgG, horseradish peroxidase (HRP)-linked whole antibody (Amersham Biosciences), anti-goat IgG-peroxidase (Sigma-Aldrich), Alexa Fluor 680 rabbit anti-mouse IgG (Invitrogen). Rabbit antiserum (RS-2) were raised against the kinase insert domain of rat VEGFR-2. It cross-reacts efficiently with the human VEGFR-2 (22).

VEGF-A165 was from PeproTech EC Ltd., VEGF-A121 was from R&D Systems, and VEGF-A145 was from Relia-Tech. VEGF-A165b was produced as described (23).

Tissue culture. Porcine aortic endothelial (PAE)/VEGFR-2 cells have been described before (24). PAE/NRP1 cells (16) were kindly provided by Dr. Michael Klagsbrun (Vascular Biology Program/Department of Surgery, Children's Hospital and Harvard Medical School, Boston, MA). PAE/VEGFR-2 and NRP1 cells were established by transfection of PAE/VEGFR-2 cells with human NRP1 cDNA in pcDNA3.1 (a kind gift from Dr. Michael Klagsbrun) mixed with pSuper.retro.puro (OligoEngine) using Lipofectamine (Invitrogen). Telomerase-immortalized dermal microvascular (TIME) cells, a kind gift from Dr. Martin McMahon (Cancer Research Institute, University of California, San Francisco, CA), and human umbilical vein endothelial cells (HUVEC), purchased from the American Type Culture Collection, were cultured on gelatinized tissue culture dishes in endothelial basal medium MV2 with growth supplements (PromoCell). Mouse aortic endothelial (MAE) cells were a kind gift from Dr. Lars Holmgren (Cancer Center Karolinska, Karolinska Institute, Stockholm, Sweden). MAE/VEGFR-2 cells were established by infection of MAE cells with lentivirus encoding mouse VEGFR-2 (see ref. 25 for creation of VEGFR-2 lentivirus). R1/SVJ 129 murine embryonic stem (ES) cells were kindly provided by Dr. Andras Nagy (Samuel Lunenfeld Research Institute, Mount Sinai Hospital, Toronto, Ontario, Canada).

Competitive binding assay. Subconfluent, serum-starved cells in 24-well plates were incubated for 2 h on ice with 0.1 μCi/mL ^{125}I-VEGF-A165 (Amersham Biosciences) with or without 1- to 1,000-fold concentration of nonlabeled competitor in triplicate conditions. Cells were washed and lysed in 20 mmol/L Tris-HCl (pH 7.5), 1% Triton X-100, and 10% glycerol, and cell-bound radioactivity was determined. Data are presented as mean ± SD.

Filter binding assay. HS was purified from PAE/VEGFR-2 cells metabolically labeled with [^{35}S]radionuclide (Perkin-Elmer). Triplicate samples of 26.2 nmol/L of each VEGF ligand were incubated with 6,000 cpm [^{35}S]HS in 200 μL PBS for 15 min and passed through a nitrocellulose filter using a multiwell vacuum-assisted filtration apparatus. After eliminating unbound [^{35}S]HS, filters were incubated in 2 mol/L NaCl to dissociate the HS from the filter. The radioactivity of protein-bound [^{35}S]HS was determined using a Wallac 1414 liquid scintillation counter (Perkin-Elmer).

Immunoprecipitation/immunoblotting. Cells were lysed in 1% NP40 and processed for immunoprecipitation/immunoblotting as described before (24). Proteins separated by SDS-PAGE were transferred to nitrocellulose (Hybond-C Extra, Amersham Biosciences) or polyvinylidene difluoride membranes (Immobilon-FL, Millipore), blocked in 5% bovine serum albumin (BSA)/PBS, 0.2% Tween 20, followed by incubation with primary and HRP-conjugated secondary antibodies in 1% BSA/PBS, 0.2% Tween 20. Blots were developed using ECL (Amersham Biosciences) and exposure to Hyperfilm ECL (Amersham Biosciences). For fluorescent blotting, samples were blocked in Blocking buffer (LI-COR) and incubated with primary and fluorescence-conjugated secondary antibodies in 0.2% Tween 20/Blocking buffer. Fluorescence was scanned using an Odyssey IR imaging system (LI-COR). Densitometric analysis of fluorographs was performed using the ImageJ 1.31 software.[3]

Chemotaxis assay. Boyden chamber migration assays were performed as previously described (24). Serum-starved cells were applied to the upper wells of the chemotaxis chamber at 25,000 per well and allowed to migrate through collagen-coated 8-μm pore polycarbonate filters (Whatman) toward the lower wells, filled with 0 to 30 nmol/L of the different ligands. Five hours later, migrating cells were fixed in methanol and stained with Giemsa. The number of migrating cells was determined using the Easy Image Analysis software (Rainfall). Samples were analyzed in at least six wells per condition at repeated occasions. Data are shown as mean ± SD.

DNA synthesis assay. [^{3}H]Thymidine incorporation assay was performed as described before (24). TIME cells were plated on gelatin-coated 24-well dishes in triplicate samples and incubated with 10 to 1,000 pmol/L VEGF-A ligands for 16 h. [Methyl-^{3}H]thymidine (1 μCi/mL; Amersham Biosciences) was added and cells were incubated for additional 6 h. Cells were washed with PBS on ice and treated with 10% trichloroacetic acid for 20 min to precipitate DNA. After rinsing with 99% ethanol, precipitated DNA was solubilized in 0.2 mol/L NaOH. Incorporated radioactivity was measured in a Wallac 1414 liquid scintillation counter. Data are shown as mean ± SD.

Peroxidase/immunofluorescent staining of EBs. ES cells were induced to differentiate by omitting leukemia inhibitory factor from the medium and aggregated in hanging drops to create EBs (26). For peroxidase staining, EBs in two-dimensional cultures (i.e., on glass culture slides) were fixed in zinc fix solution [0.1 mol/L Tris-HCl (pH 7.5), 3 mmol/L calcium acetate, 23 mmol/L zinc acetate, 37 mmol/L zinc chloride, containing 0.2% Triton X-100], treated with 3% H_2O_2 to suppress endogenous peroxidase activity, and blocked in TBS/0.1% Tween 20/3% BSA (BSA/TBS-t). Samples were incubated with primary rat anti-mouse CD31 antibody (BD Biosciences) and biotinylated anti-rat IgG (Vector Laboratories) in BSA/TBS-t followed by incubation with HRP-conjugated streptavidin (Vector Laboratories) and the chromogen substance (AEC Substrate Kit For Peroxidase, Vector Laboratories). Mounting was done using Ultramount aqueous permanent mounting medium (Dako). For fluorescent staining, three-dimensional cultured EBs (i.e., in a three-dimensional collagen gel) were fixed in 4% paraformaldehyde/TBS, blocked, and permeabilized in TBS/0.2% Triton X-100/3% BSA. Samples were incubated with primary rat anti-mouse CD31 antibody and Alexa Fluor 555 goat anti-rat IgG (Invitrogen) in BSA/TBS-t and inspected using either a Nikon Eclipse E1000 microscope with a Nikon Eclipse DXM 1200 camera (Nikon).

Matrigel plug assay. Animal work was approved by the Uppsala university board of animal experimentation. Six-week-old female nude mice were anesthetized using isoflurane (Forene, Abbott) and s.c. injected with 350 μL Matrigel (BD Biosciences) supplemented with sphingosine-1-phosphate (S1P, Avanti Polar Lipids) with or without 130 nmol/L VEGF-A ligands. Mice were euthanized 7 d later and Matrigel plugs were retrieved and fixed in 4% paraformaldehyde followed by whole mount staining. The angiogenic response was detected by immunostaining using rat anti-mouse CD31 and mouse monoclonal anti-α-smooth muscle actin (α-SMA)-FITC conjugate (Sigma-Aldrich) followed by incubation with Alexa Fluor 594 donkey anti-rat IgG (Invitrogen). Samples were analyzed using a Zeiss LSM 510 META confocal microscope. For each condition, three to six Matrigel plugs were inspected at two independent occasions. Vessel branch points were marked and counted manually (n = 5 for each condition). Data are shown as mean ± SD.

Two-dimensional phosphopeptide mapping. MAE/VEGFR-2 cells were serum starved and pretreated with 5 μg/mL anti-VEGF antibody (R&D Systems) in 0.1% BSA/Ham's F-12 medium overnight to block endogenous VEGF-A. Cells were washed and then stimulated with 3 nmol/L VEGF-A ligands for 5 min and processed for immunoprecipitation with

[3] http://rsb.info.nih.gov/ij/download.html

anti-mouse VEGFR-2 (R&D Systems) followed by labeling using [γ-^{32}P]ATP (Amersham Biosciences) in a kinase reaction as described previously (27). ^{32}P-labeled phosphorylated VEGFR-2 (pVEGFR-2) was separated by SDS-PAGE, transferred to a polyvinylidene difluoride membrane, and analyzed using a Bio-Imager BAS-1800II (Fujifilm). The phosphorylated receptor bands were excised and blocked with 0.5% polyvinyl pyrrolidone/0.1 mol/L acetic acid followed by digestion with trypsin (Promega) and oxidation with performic acid. Tryptic peptides were applied to cellulose TLC plates (Merck) for two-dimensional separation, electrophoresis in pH 1.9 buffer (2.2% formic acid, 7.8% acetic acid) using a Hunter thin-layer electrophoresis apparatus (C.B.S. Scientific) for 40 min at 2,000 V, and ascending chromatography in isobutyric acid buffer (62.5% isobutyric acid, 1.9% *n*-butyl alcohol, 4.8% pyridine, and 2.9% acetic acid) overnight. The radioactivity of separated ^{32}P-labeled peptides was analyzed using the Bio-Imager equipment.

Results

Binding of VEGF-A165, VEGF-A165b, VEGF-A121, and VEGF-A145 to VEGFR-2, NRP1, and HS. To determine the properties of VEGF-A165b, we compared the abilities of the different VEGF isoforms, VEGF-A165, VEGF-A165b, VEGF-A145, and VEGF-A121, to interact with VEGFR-2 and the coreceptors NRP1 and HS. As a model, we used PAE cells. PAE cells lack endogenous expression of both VEGFR-2 and NRP1 (16, 22) but were stably transfected to express the human VEGFR-2 alone or VEGFR-2 together with NRP1. Figure 1*A* shows immunoblotting to detect expression of VEGFR-2 and NRP1 in the different PAE cells. Parallel immunoblotting of primary HUVECs showed comparable expression levels in the transfected PAE cells and the primary endothelial cells, although the PAE/VEGFR-2, NRP1 cells expressed higher levels of NRP1 than did HUVECs. Interactions of ligands with VEGFR-2 and NRP1 were analyzed through competition assays using ^{125}I-VEGF-A165 for binding to different PAE cell lines. Untransfected PAE cells bound only low levels of ^{125}I-VEGF-A165 in a manner that could not be competed out by unlabeled VEGF-A165 (data not shown), in agreement with that these cells express neither VEGFR-2 nor NRP1 endogenously (16, 22, 28).

All tested VEGF-A ligands, including VEGF-A165b, competed for binding of ^{125}I-VEGF-A165 to PAE/VEGFR-2 cells, although VEGF-A165b and VEGF-A121 competed less efficiently than VEGF-A165 and VEGF-A145 (Fig. 1*B*). VEGF-A165b and VEGF-121 failed to

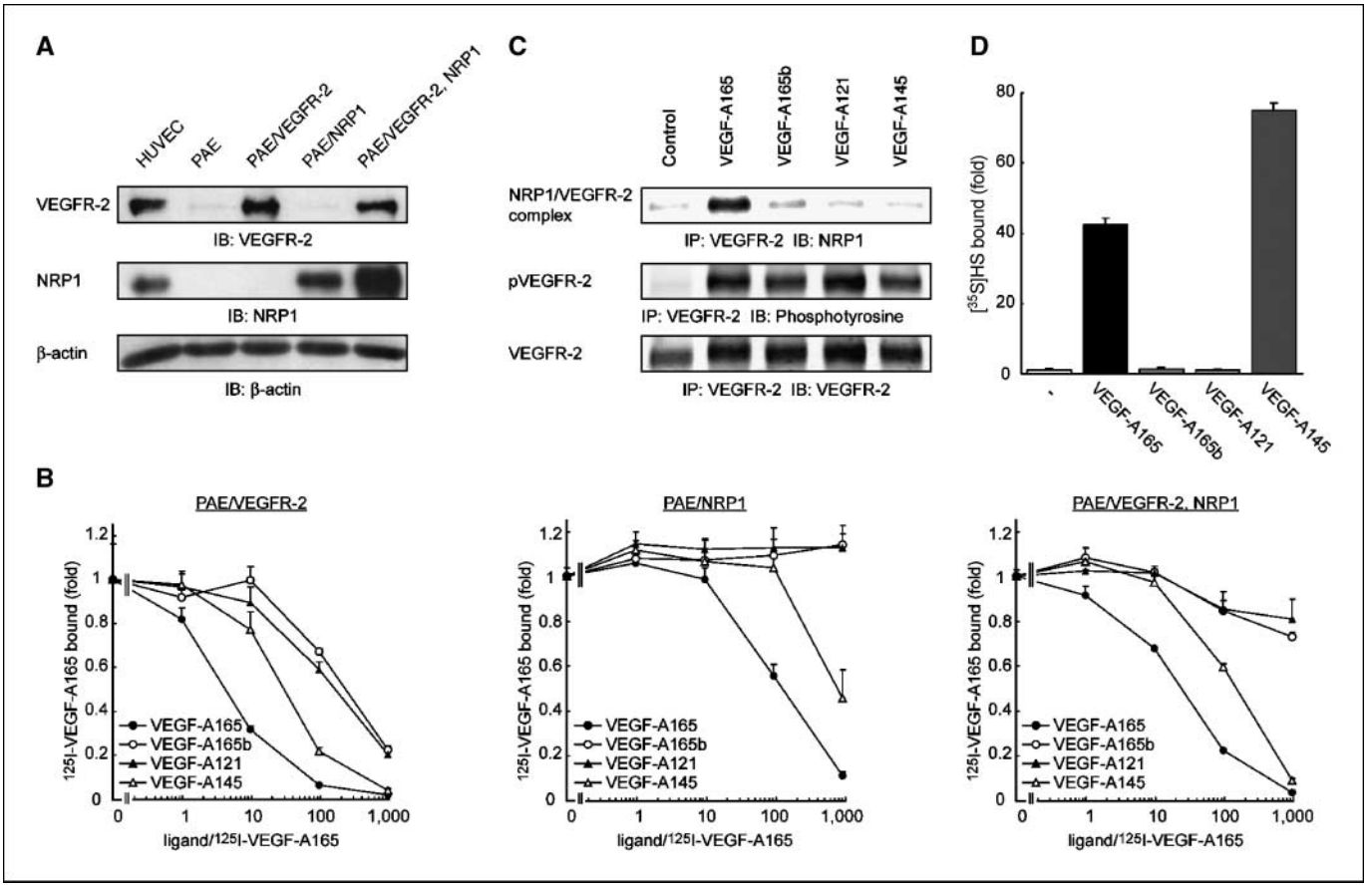

Figure 1. Interaction of different VEGF isoforms with VEGFR-2, HS, and NRP1. *A,* immunoblotting of primary HUVECs, untransfected PAE, and PAE cells expressing VEGFR-2 alone (PAE/VEGFR-2), NRP1 alone (PAE/NRP1), or both (PAE/VEGFR-2 and NRP1). Blotting was performed on total cell lysates with antibodies against VEGFR-2 (*top*), NRP1 (*middle*), and, as a control for equal loading, β-actin (*bottom*). *B,* competition assays on the different PAE cell lines using ^{125}I-VEGF-A165. *Left,* ^{125}I-VEGF-A165 binding to PAE/VEGFR-2 cells was competed by unlabeled VEGF-A165, VEGF-A165b, VEGF-A121, or VEGF-A145, indicating binding of all four VEGF ligands to VEGFR-2. *Middle,* ^{125}I-VEGF-A165 binding to PAE/NRP1 cells was effectively competed by unlabeled VEGF-A165 and by a 1,000-fold molar excess of VEGF-A145 but not by VEGF-A165b or VEGF-A121. This suggests efficient binding of VEGF-A165 and very low affinity binding of VEGF-A145 to NRP1 but no binding of VEGF-A165b or VEGF-A121 to NRP1. *Right,* ^{125}I-VEGF-A165 binding to PAE/VEGFR-2 and NRP1 cells showed competition by all ligands. *C,* the extent of VEGFR-2/NRP1 complex formation was assessed by immunoprecipitation (*IP*) of VEGFR-2 followed by immunoblotting (*IB*) for NRP1 in PAE/VEGFR-2 and NRP1 cells treated with 2 nmol/L VEGF-A isoforms for 5 min. Only VEGF-A165 induced detectable VEGFR-2/NRP1 complex formation. *Middle,* tyrosine phosphorylation of VEGFR-2; *bottom,* loading of the receptor. *D,* [^{35}S]HS retention on nitrocellulose filter as a consequence of specific binding to VEGF-A variants was examined. [^{35}S]HS was retained by binding to VEGF-A165 and even more efficiently to VEGF-A145. In contrast, [^{35}S]HS did not bind to VEGF-A165b or VEGF-A121.

compete for binding to cells expressing NRP1 alone. VEGF-A145 showed competition for binding to NRP1, although a 1,000-fold molar excess of VEGF-A145 was needed, indicating very low affinity. VEGF-A145 lacks the NRP1-binding exon 7, but exon 8 in the *vegf-a* gene has also been implicated in binding to NRP1 (10).

In PAE cells coexpressing VEGFR-2 and NRP1, competition by VEGF-A165b and VEGF-A121 for binding of ^{125}I-VEGF-A165 was less efficient than for PAE/VEGFR-2 cells. This agrees with that VEGF-A165 binds efficiently to NRP1, whereas VEGF-A165b and VEGF-A121 do not. Again, VEGF-A145 competed, although inefficiently, with the radiolabeled ligand.

Next, the ability of the ligands to induce complex formation between VEGFR-2 and NRP1 was tested. PAE cells expressing both VEGFR-2 and NRP1 were treated with the different VEGF-A isoforms and NRP1/VEGFR-2 complex formation was examined by immunoprecipitation of VEGFR-2 and immunoblotting to detect NRP1. As shown in Fig. 1*C*, all ligands induced VEGFR-2 tyrosine phosphorylation. Immunoblotting showed that VEGF-A165 induced potent complex formation between VEGFR-2 and NRP1. In contrast, VEGF-A165b, VEGF-A121, and VEGF-A145 failed to induce detectable complex formation between NRP1 and VEGFR-2, in agreement with that the affinity for binding to NRP1 was low for these factors (see Fig. 1*B*).

The binding ability of VEGF-A variants to HS was determined through use of a nitrocellulose filter binding assay (29), in which metabolically labeled, purified [^{35}S]HS is retained only when bound to a growth factor. As shown in Fig. 1*D*, VEGF-165b as well as VEGF-A121 failed to retain labeled HS, whereas VEGF-A145 retained HS more efficiently than VEGF-A165.

Our data indicate that the binding ability of VEGF-A165b to coreceptors is similar to that of VEGF-A121 as both fail to bind to NRP1 as well as to HS. In contrast, VEGF-A165 binds strongly to both, whereas VEGF-A145 binds strongly to HS and weakly to NRP1.

VEGFR-2 activation by the VEGF ligands. We next examined the concentration-dependent activation of VEGFR-2 in the presence and absence of NRP1 by the different VEGF ligands. Figure 2*A* shows that VEGF-A165–induced activation of VEGFR-2 in PAE/VEGFR-2 cells was discernible at 0.1 nmol/L of the ligand. Tyrosine phosphorylation reached a maximal level at 1 nmol/L of VEGF-A165, whereafter it decreased slightly. A higher concentration, 0.3 to 1 nmol/L, was required for the other three ligands,

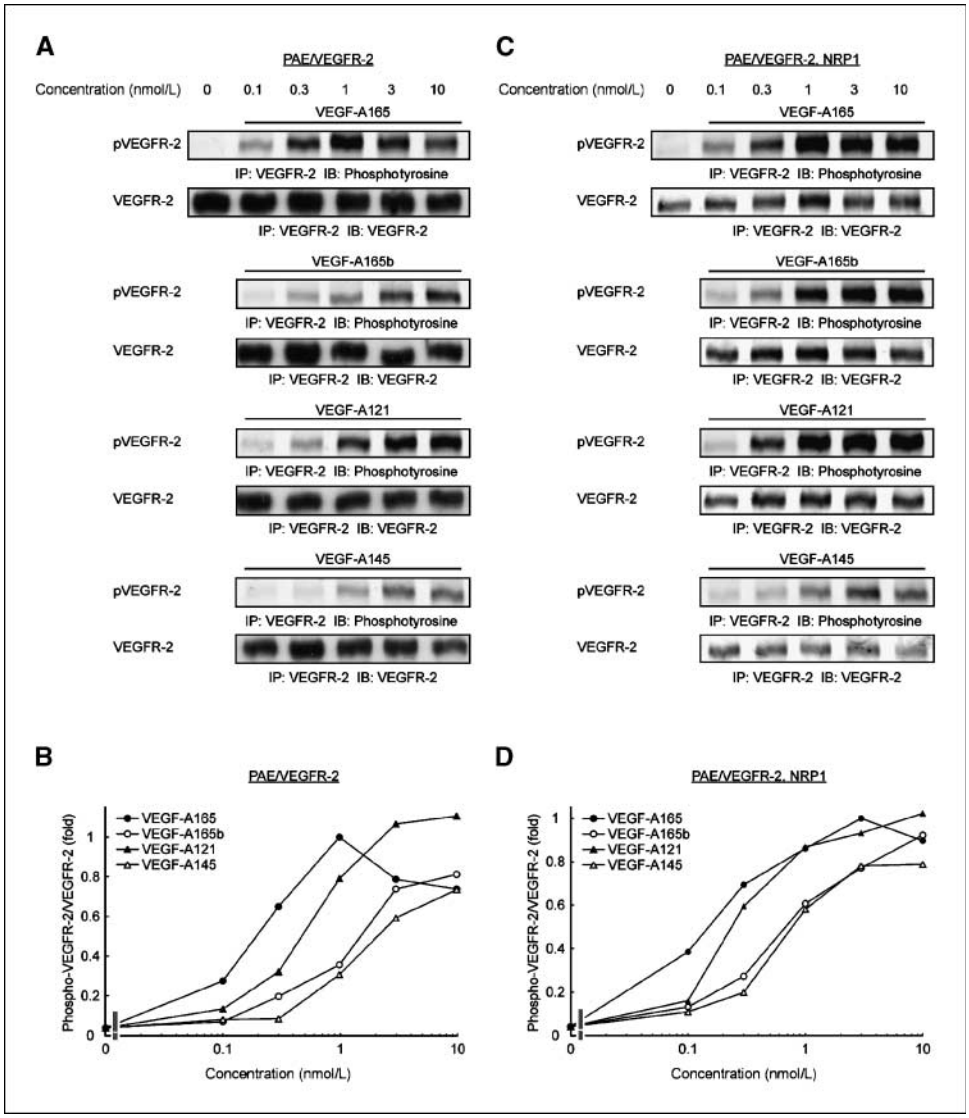

Figure 2. Dose response of VEGF-A ligands in tyrosine phosphorylation of VEGFR-2. *A*, response to a dose range of 0.1 to 10 nmol/L of VEGF-A165, VEGF-A165b, VEGF-A121, or VEGF-A145 as indicated. Cells were treated with VEGF ligands for 5 min, lysed and processed for immunoprecipitation (*IP*) followed by immunoblotting (*IB*) for phosphotyrosine or VEGFR-2 to detect pVEGFR-2 or VEGFR-2 protein, respectively. *B*, quantification of pVEGFR-2/VEGFR-2 shown in *A*. Peak phosphorylation of VEGFR-2 induced by VEGF-A165 was set to 1. *C*, dose response of VEGFR-2 phosphorylation in PAE/VEGFR-2, NRP1 cells to the same range of concentrations of VEGF-A ligands as in *A*. *D*, quantification of pVEGFR-2/VEGFR-2 shown in *C*. Maximum induction of VEGF-A165 was set to 1.

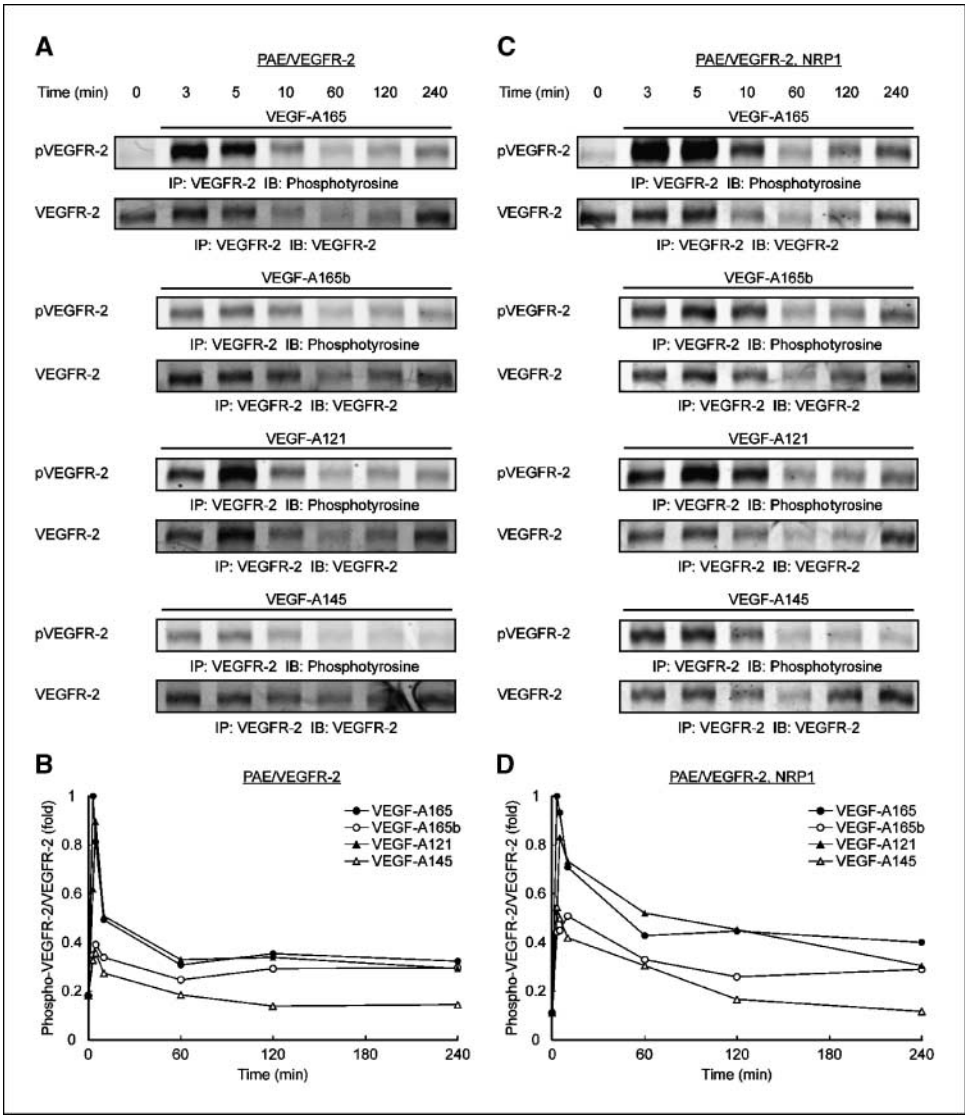

Figure 3. Kinetics of VEGFR-2 phosphorylation by VEGF-A ligands. *A,* PAE/VEGFR-2 cells treated with 1 nmol/L of VEGF-A165, VEGF-A165b, VEGF-A121, or VEGF-A145 for 3 to 240 min were examined for kinetics of VEGFR-2 phosphorylation. *B,* quantification of pVEGFR-2/VEGFR-2 shown in *A*. Peak induction of VEGF-A165 was set to 1. *C*, PAE/VEGFR-2 and NRP1 cells treated with 1 nmol/L each of the different VEGF-A isoforms. *D,* quantification of pVEGFR-2/VEGFR-2 shown in *C*. Maximum phosphorylation of VEGFR-2 induced by VEGF-A165 was set to 1.

VEGF-A165b, VEGF-A121, and VEGF-A145, to induce VEGFR-2 tyrosine phosphorylation. Maximal receptor tyrosine phosphorylation also required higher concentrations of these ligands and was achieved at 3 to 10 nmol/L (see quantification of pVEGFR-2/VEGFR-2 in Fig. 2*B*). Overall, the concentration-dependent pattern of VEGFR-2 tyrosine phosphorylation was similar between all VEGF isoforms studied, although VEGF-A145 and VEGF-A165b consistently performed less efficiently than VEGF-A121 and VEGF-A165.

A similar pattern was seen in PAE/VEGFR-2, NRP1 cells; VEGF-A165 and VEGF-A121 induced more potent VEGFR-2 tyrosine phosphorylation (set in relation to the total VEGFR-2 pool) than VEGF-A165b and VEGF-A145 (Fig. 2*C* and *D*).

We also examined the kinetics of VEGFR-2 phosphorylation. PAE/VEGFR-2 cells and PAE/VEGFR-2, NRP1 cells were treated with the VEGF-A ligands for 3 to 240 min. As shown in Fig. 3*A* and *C* (quantification in Fig. 3*B* and *D*), the kinetics of receptor phosphorylation showed the same pattern for all ligands and was only very moderately affected by expression of NRP1. Thus, VEGFR-2 tyrosine phosphorylation was induced within 5 min and diminished again after 10 min. The decrease in phosphorylation was due both to dephosphorylation by phosphotyrosine phosphatases and to internalization and degradation of receptors (detected as clearance of receptor protein; see immunoblots for VEGFR-2) followed by restoration of receptor expression by new synthesis and export of receptors to the cell surface. For a review on ligand-induced VEGFR activation and internalization, see ref. 5. For the time course studied, we detected only subtle differences between the different VEGF isoforms in kinetics of VEGFR-2 phosphorylation.

In conclusion, VEGF-A165b is able to induce VEGFR-2 tyrosine phosphorylation in a dose-dependent manner with kinetics similar to that of VEGF-A121 and only slightly less efficiently than VEGF-A165.

Ability of VEGF ligands to induce endothelial cell responses *in vitro*. To determine the biological activity *in vitro* of VEGF-A165b, we analyzed the chemoattractive effects of the VEGF ligands. PAE/VEGFR-2 cells migrated toward VEGF-A165, VEGF-A165b, and VEGF-A121 with similar efficiency. In the presence of NRP1 (i.e., using PAE/VEGFR-2, NRP1 cells), VEGF-A165–induced endothelial cell migration was enhanced, whereas the migration induced by VEGF-A165b or VEGF-A121 was not affected by

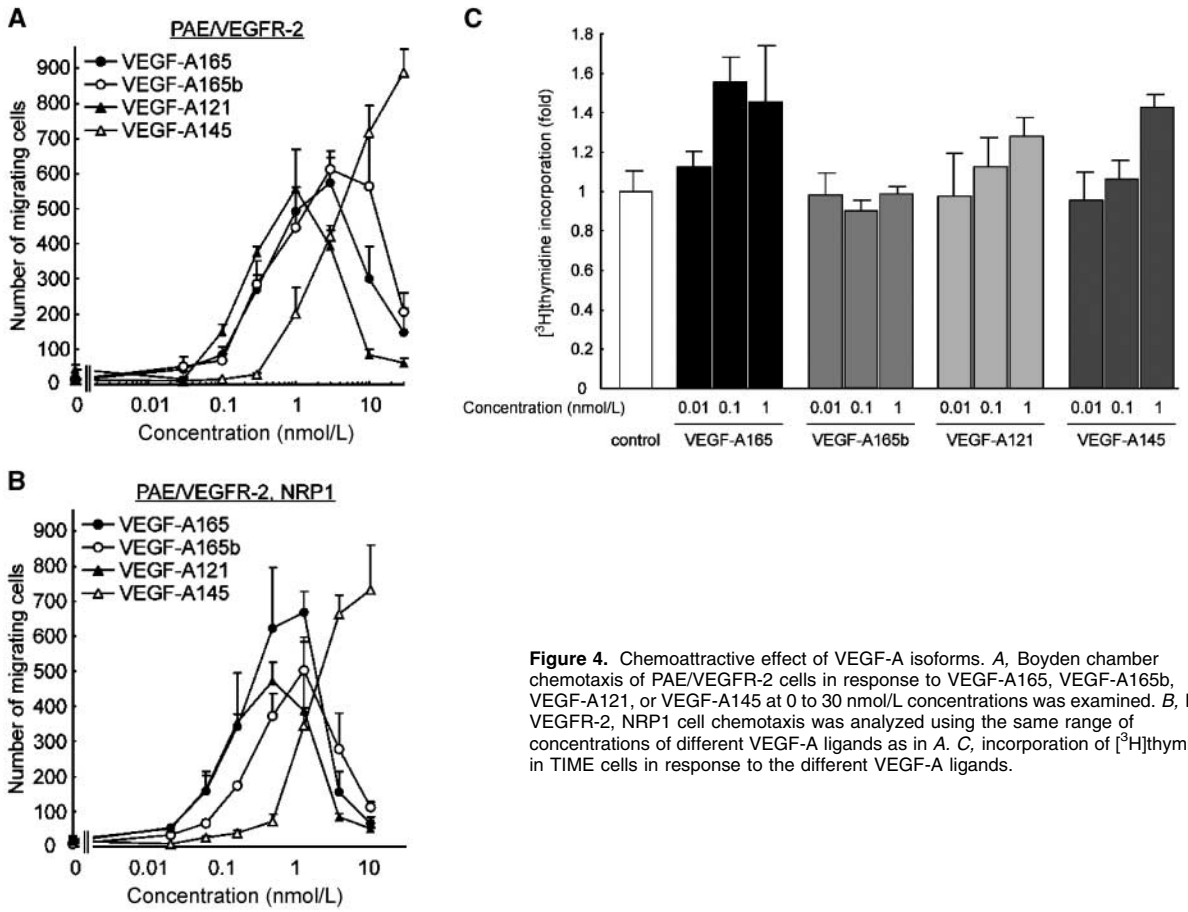

Figure 4. Chemoattractive effect of VEGF-A isoforms. *A,* Boyden chamber chemotaxis of PAE/VEGFR-2 cells in response to VEGF-A165, VEGF-A165b, VEGF-A121, or VEGF-A145 at 0 to 30 nmol/L concentrations was examined. *B,* PAE/VEGFR-2, NRP1 cell chemotaxis was analyzed using the same range of concentrations of different VEGF-A ligands as in *A. C,* incorporation of [^{3}H]thymidine in TIME cells in response to the different VEGF-A ligands.

expression of NRP1. This agrees with the finding that VEGF-A165b and VEGF-A121 do not bind NRP1. VEGF-A145 showed a unique pattern in the migration assays using either PAE/VEGFR-2 or PAE/VEGFR-2, NRP1 cells, as shown in Fig. 4*A* and *B*. Strikingly, VEGF-A145 did not induce the typical bell-shaped curve with reduced migration at higher concentrations. It is possible that the very high affinity for binding to HS (see Fig. 1*D*) influenced the readout of VEGF-A145 effects in this assay. Thus, we find that VEGF-A165b is a chemoattractant for cells expressing VEGFR-2, irrespective of expression of NRP1.

Next, we tested the ability of the VEGF ligands to stimulate incorporation of [^{3}H]thymidine in TIME cells (Fig. 4*C*). We chose TIME cells for this assay because PAE cells are transformed and therefore not suitable for testing effects on mitogenicity. VEGF-A165, VEGF-A121, and VEGF-A145 induced significant effects when given at a concentration of 1 nmol/L. In contrast, VEGF-A165b did not stimulate [^{3}H]thymidine incorporation.

In conclusion, VEGF-A165b induces VEGFR-2 activation and short-term endothelial responses such as chemotaxis (5-h duration). The ability of VEGF-A165b to perform in a more long-term assay, such as endothelial cell DNA synthesis (24 h), was, however, severely hampered when compared with other VEGF ligands.

Endothelial cell plexus formation in differentiating ES cells. To test the angiogenic activity of VEGF-A165b compared with the other VEGF ligands in a more complex model, we used differentiating mouse ES cells, EBs. Hallmarks of vasculogenesis and angiogenesis are faithfully recapitulated in the EBs subjected either to two-dimensional cultures or to culture in a three-dimensional collagen matrix (26). We previously showed that day 10 EBs (i.e., differentiated for 10 days) express NRP1 and HS, which colocalize with VEGFR-2 in endothelial cells.[4]

Two-dimensional EB cultures treated with VEGF-A165 displayed the typical vascular plexus in the periphery of cultures (Fig. 5*A, top middle*; high magnification in the *top right*). In contrast, VEGF-A165b failed to induce formation of vessel structures. Similarly, treatment with VEGF-A121 and VEGF-A145 did not lead to plexus formation of endothelial cells in the two-dimensional cultures. It is noteworthy that although VEGF-A165b and VEGF-A121 lacked HS-binding ability, this cannot explain their inability to induce a vascular plexus, as VEGF-A145, which binds strongly to HS (see Fig. 1*D*), also failed to induce plexus formation.

The ability of the VEGF-A ligands to induce formation of angiogenic sprouts was determined in three-dimensional cultures of EBs. As shown in Fig. 5*B* (*top middle*; high magnification in the *top right*), VEGF-A165 induced vascular sprouts that invaded into the collagen matrix. The other VEGF ligands, however, induced very few short sprouts, if any at all.

[4] H. Kawamura, X. Li, et al., submitted for publication.

Next, the different VEGF-A ligands were mixed with Matrigel and the mixtures were injected s.c. in nude mice. As shown in Fig. 5*C*, inclusion of VEGF-A165 induced abundant vascularization of the Matrigel with richly branched, pericyte-covered vessels. In contrast, inclusion of VEGF-A165b led to invasion of endothelial cells into the Matrigel, but the cells failed to organize into vessels and also failed to attract pericytes. In the VEGF-A121–containing Matrigel plugs, occasional vessel structures were seen, which lacked branch points and a pericyte coat. In VEGF-A145–containing Matrigel plugs, branching, pericyte-clad vessels were seen but to a much

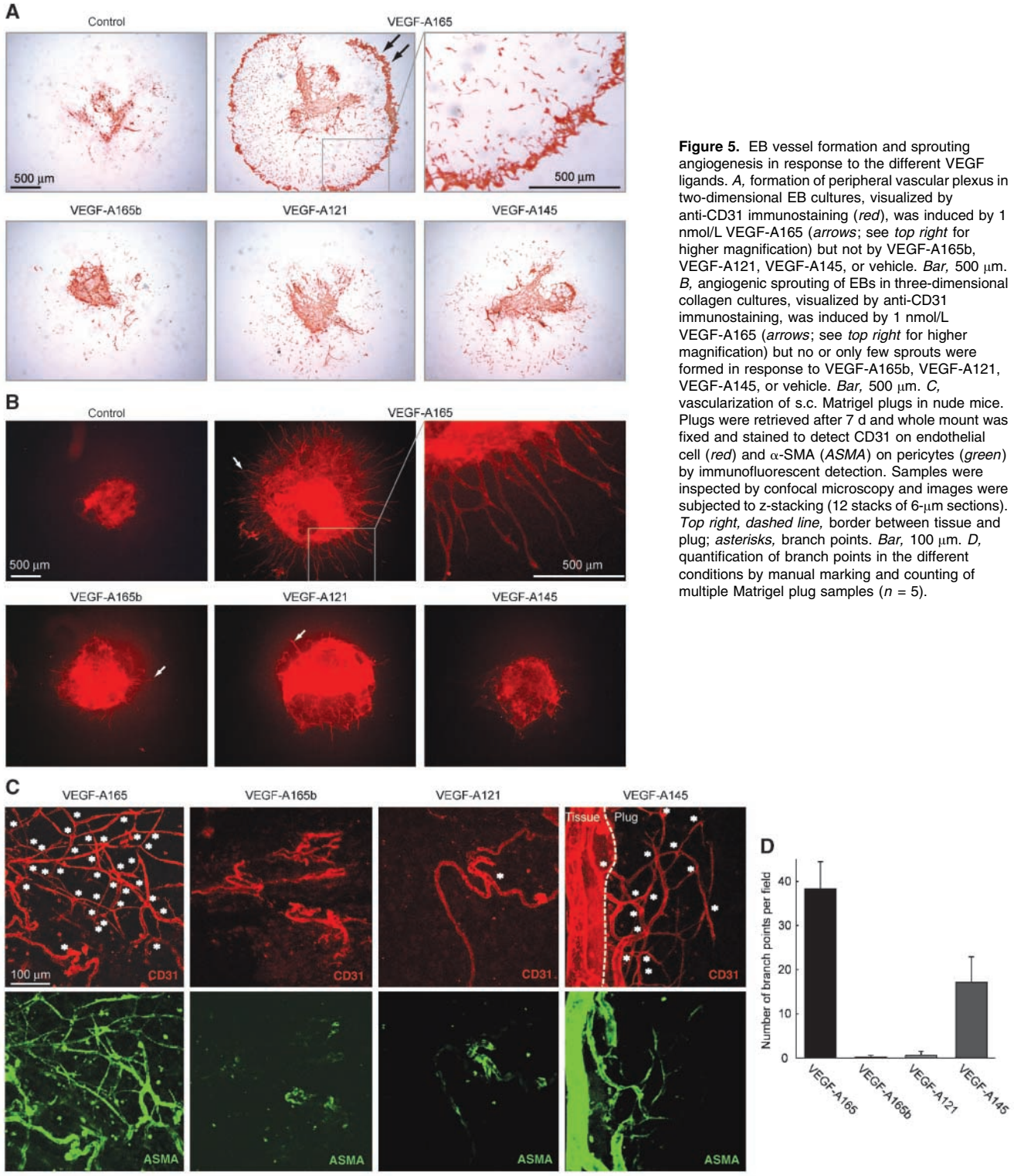

Figure 5. EB vessel formation and sprouting angiogenesis in response to the different VEGF ligands. *A,* formation of peripheral vascular plexus in two-dimensional EB cultures, visualized by anti-CD31 immunostaining (*red*), was induced by 1 nmol/L VEGF-A165 (*arrows*; see *top right* for higher magnification) but not by VEGF-A165b, VEGF-A121, VEGF-A145, or vehicle. *Bar,* 500 μm. *B,* angiogenic sprouting of EBs in three-dimensional collagen cultures, visualized by anti-CD31 immunostaining, was induced by 1 nmol/L VEGF-A165 (*arrows*; see *top right* for higher magnification) but no or only few sprouts were formed in response to VEGF-A165b, VEGF-A121, VEGF-A145, or vehicle. *Bar,* 500 μm. *C,* vascularization of s.c. Matrigel plugs in nude mice. Plugs were retrieved after 7 d and whole mount was fixed and stained to detect CD31 on endothelial cell (*red*) and α-SMA (*ASMA*) on pericytes (*green*) by immunofluorescent detection. Samples were inspected by confocal microscopy and images were subjected to z-stacking (12 stacks of 6-μm sections). *Top right, dashed line,* border between tissue and plug; *asterisks,* branch points. *Bar,* 100 μm. *D,* quantification of branch points in the different conditions by manual marking and counting of multiple Matrigel plug samples ($n = 5$).

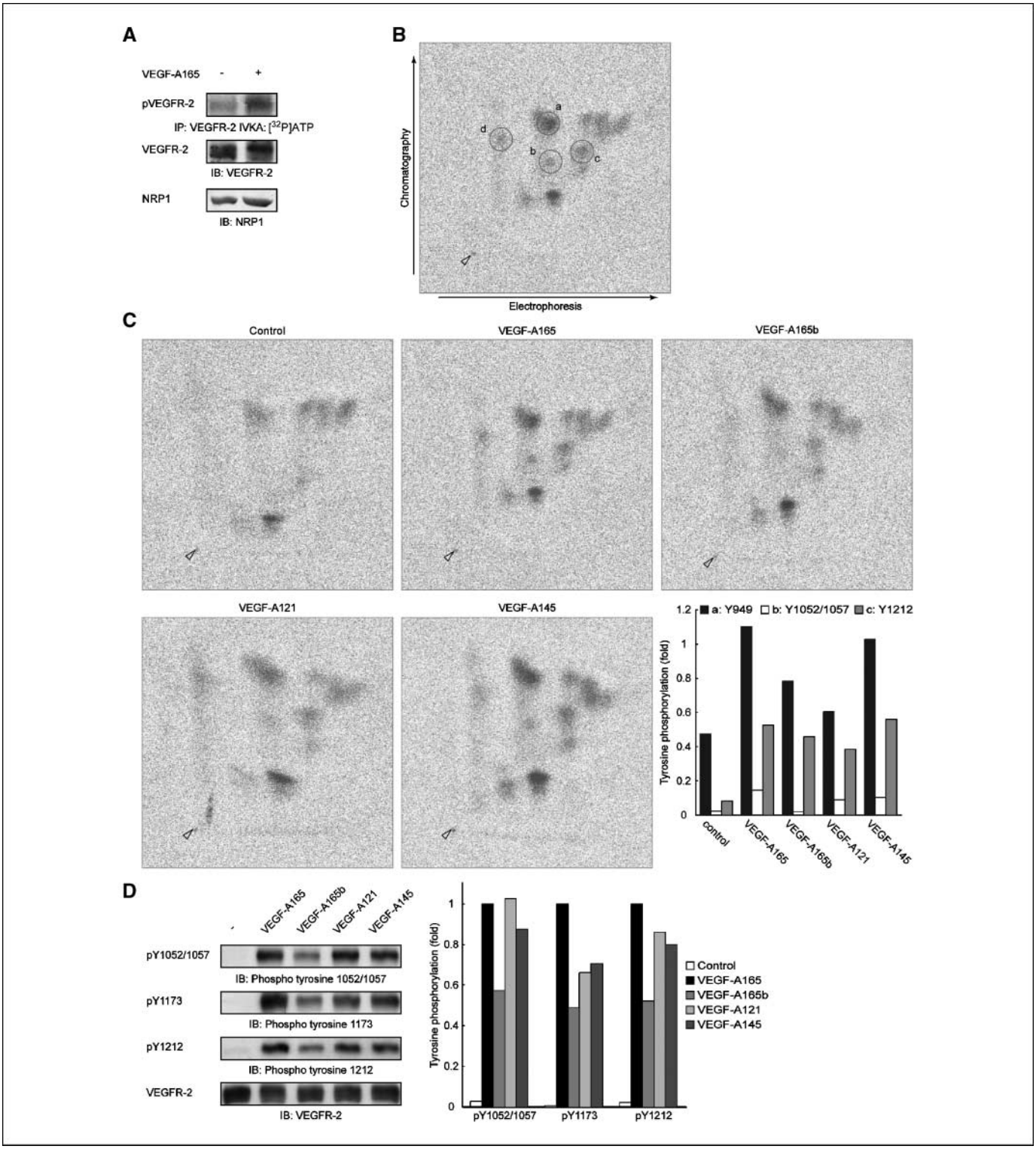

Figure 6. Phosphorylation of tyrosine residues in VEGFR-2 by VEGF-A ligands. *A,* MAE cells transfected to enhance mouse VEGFR-2 expression were used for mapping of tyrosine phosphorylation sites in VEGFR-2. Cells were treated with 3 nmol/L VEGF-A ligands for 5 min followed by labeling of VEGFR-2 by *in vitro* kinase assay using [γ-^{32}P]ATP. Endogenous expression of NRP1 in MAE cells was shown by immunoblotting. *B,* tryptic digests of ^{32}P-labeled VEGFR-2 immunoprecipitated from MAE/VEGFR-2 cells treated with vehicle or with the different VEGF-A isoforms were separated by electrophoresis and chromatography on a cellulose TLC plate. The plate was exposed on a Bio-Imager to visualize the position of the different VEGFR-2 phosphopeptides. *Arrowhead,* position of sample application on the plate. *a* to *d,* phosphopeptide spots induced by VEGF-A stimulation (see ref. 22). *a,* Y949 (Y951 in human sequence); *b,* Y1052 (Y1054); *c,* Y1212 (Y1214); *d,* a serine/threonine phosphorylation site. Y1173, another major tyrosine phosphorylation site of VEGFR-2, could not be identified due to the negative charge of the 1173-containing tryptic peptide under the used condition. *C,* induction of phosphopeptides by treatment of MAE/VEGFR-2 cells with the different VEGF-A isoforms. *Bottom right,* quantification of ^{32}P peptides. *D,* MAE/VEGFR-2 cells treated with 3 nmol/L VEGF-A isoforms for 5 min were examined for phosphorylation of Y1052/Y1057, Y1173, and Y1212 in VEGFR-2 by immunoblotting using phosphotyrosine site-specific antibodies. *Right,* quantification of phosphorylated tyrosine sites. Induction of VEGF-A165 was set to 1.

lesser extent than in the VEGF-A165–containing Matrigel plugs. Figure 5*D* shows quantification of the number of branch points in the different conditions. We conclude that the *in vivo* phenotypes of each of the tested VEGF-A isoforms differed and the degree of response to VEGF-A165 was not matched by any of the other isoforms. It is noteworthy that VEGF-A121 and VEGF-A165b, which both completely lack NRP1 binding, failed to induce endothelial cell/pericyte association. Both these ligands also lack HS-binding ability, which may contribute to the lack of response. However, VEGF-A145, which binds potently to HS and with low affinity to NRP1 (see Fig. 1), performed poorly compared with VEGF-A165.

Differential usage of tyrosine phosphorylation sites in VEGFR-2 by VEGF-A165b. We asked whether the molecular mechanisms underlying the inability of certain VEGF ligands to perform in the angiogenesis assays involved changes in VEGFR-2–dependent signal transduction. Because signal transduction is dependent on activation of VEGFR-2 leading to autophosphorylation on tyrosine residues, we mapped VEGFR-2 phosphorylation site usage in response to the different ligands. For this purpose, we used mouse aortic endothelial (MAE) cells transfected to enhance mouse VEGFR-2 expression. Immunoblotting showed functional VEGFR-2 and endogenous NRP1 expression on MAE cells (Fig. 6*A*). This cell line was chosen because it showed lower phosphorylation of VEGFR-2 under basal conditions compared with other cell lines tested (PAE/VEGFR-2, NRP1 cells and 293 cells) most likely due to less production of endogenous VEGF. Still, the cells were treated with neutralizing VEGF antibodies overnight to block the effect of endogenous VEGF production. After washing and acute treatment of cells with different VEGF-A isoforms, immunoprecipitated VEGFR-2 was labeled using [γ-^{32}P]ATP in a kinase reaction (Fig. 6*A*); we have shown that this procedure faithfully mimics phosphorylation in intact cells (30). The ^{32}P-labeled VEGFR-2 was isolated and digested with trypsin followed by two-dimensional separation through electrophoresis and liquid chromatography.

As shown in Fig. 6*B*, VEGF-A stimulation induced several phosphorylated tyrosine spots, indicated as spots *a* to *d* in the figure. We have previously identified the tyrosine sites corresponding to each of these spots by amino acid sequence and by phosphopeptide mapping using mutated VEGFR-2 with exchange of tyrosine to phenylalanine residues at individual sites. Thereby, we have shown that spots *a, b*, and *c* correspond to Y949 (Y951 in the human sequence), Y1052 (Y1054), and Y1212 (Y1214), respectively (see ref. 24). Spot *d* is a serine/threonine phosphorylation site whose amino acid sequence position has not been identified.

VEGF-A165 induced all of spots *a* to *c*, as did VEGF-A145 (Fig. 6*C*). All spots were induced by VEGF-A121 as well, although the level of induction by VEGF-A121 was lower than for VEGF-A165. VEGF-A165b induced spots *a* and *c* to a similar extent as VEGF-A121; however, the induction of spot *b* was essentially lost, indicating that VEGF-A165b only very poorly, if at all, induces phosphorylation of Y1052 in mouse VEGFR-2.

In an alternative strategy, we analyzed induction of VEGFR-2 tyrosine phosphorylation of different sites by the VEGF-A isoforms by immunoblotting using phospho-specific antibodies against Y1052/Y1057 and Y1212. In addition, we used phosphosite-specific antibodies to examine phosphorylation of Y1173, another major tyrosine phosphorylation site that is not amenable to phosphopeptide mapping using the conditions above due to the negative charge of the Y1173-containing tryptic peptide. As shown in Fig. 6*D*, Y1052/Y1057 was less efficiently phosphorylated by VEGF-A165b than by all other ligands, which is compatible with the result of phosphorylation site mapping. Phosphorylation of Y1173 was relatively poorly induced by VEGF-A165b, VEGF-A121, and VEGF-A145 compared with VEGF-A165. For Y1212, phosphorylation was more efficiently induced by VEGF-A121 and VEGF-A145 than by VEGF-A165b. We conclude that Y1052/Y1057 (corresponding to Y1054/Y1059 in the human sequence) was less efficiently phosphorylated in response to VEGF-A165b treatment than the other VEGF isoforms.

Discussion

The purpose of this study was to determine the mechanism of action of VEGF-A165b on VEGFR-2. By comparing its effects with those of other VEGF-A isoforms, we were able to unequivocally categorize VEGF-A165b as a VEGFR-2 agonist in the absence of expression of other VEGFRs. We confirm and present a mechanism for the data by Cebe Suarez and colleagues (18). Thus, like VEGF-A121, VEGF-A165b fails to bind to both NRP1 and HS, and both ligands also failed to induce vascularization in EBs as well as in s.c. Matrigel plugs. We believe that this deficiency can be explained at least in part by the lack of engagement of NRP1 in the VEGFR-2 signaling complex.

We also characterized the VEGF-A145 isoform, which lacks exons 6b and 7 in the *vegf-a* gene. Poltorak and colleagues (31) previously concluded that VEGF-145 possesses distinct biological properties. We agree with this conclusion. A marked feature of VEGF-A145 was its very strong binding to HS, 2-fold higher than that for VEGF-A165 (cf. Fig. 1*D*). Furthermore, Poltorak and colleagues showed that VEGF-A145 binds strongly to extracellular matrix, which may contribute to the enhanced endothelial cell chemotaxis observed by us (Fig. 4*A* and *B*). Still, VEGF-A145 showed only a weak angiogenic response *in vivo*, which we attribute to its poor NRP1-binding properties. Thus, HS binding alone was insufficient for induction of potent vascular organization. We conclude that VEGF-A121, VEGF-A145, and VEGF-A165b all show low or no binding to NRP1, which may account for the lack of, or strongly reduced, ability to induce endothelial cell organization and angiogenesis.

We detected a profound difference in usage of VEGFR-2 tyrosine phosphorylation sites between VEGF-A165b and the other tested VEGF-A isoforms. Both by analyzing VEGF-A165b–induced VEGFR-2–derived tryptic phosphopeptides and by use of phosphosite-specific antibodies, we detected a clear reduction in the phosphorylation of Y1052/Y1057 (human sequence Y1054/Y1059). It is noteworthy that Y1052 and Y1057 are located on the activation loop in the second part of the tyrosine kinase domain. The position of Y1057 corresponds exactly to that of the positive regulatory tyrosine residue Y416 in c-Src. Phosphorylation of the activation lip tyrosine residue(s) locks the loop in an off position, exposing the ATP-binding site and enhancing kinase activity. The loss of phosphorylation at Y1052 in VEGFR-2 seemed more profound when analyzed by phosphopeptide mapping compared with immunoblotting. This may be due to that the different phosphosite-specific antibodies bind not only to the phosphotyrosine residue but also to some extent to the surrounding amino acid residues. Moreover, the phosphosite-specific antibody detects both Y1052 and Y1057; in the VEGFR-2 phosphopeptide map, we have identified the position of the Y1052-containing peptide, but we have not been able to pinpoint the migration position of the Y1057 phosphopeptide (24). The result from the phosphosite-specific antibody can therefore not be directly compared with the

phosphopeptide mapping results. The phosphopeptide mapping is less sensitive but allows comparison of the relative stoichiometry of the different phosphosites.

In vitro, the lower stoichiometry of phosphorylation at the positive regulatory sites may not be critical because receptors are overexpressed and relatively high concentrations are used for the purified ligands. Thus, short-term responses may be relatively unaffected, whereas more long-term responses are crippled. Reduced phosphorylation at positive regulatory sites as has been described for VEGFR-1 (28) does not preclude activation of receptor tyrosine kinases but is associated with poor responsiveness.

Is the impairment in positive regulation of VEGFR-2 kinase activity by VEGF-A165b important in its antiangiogenic effect? It is possible that VEGF-A165b produced in excess would block binding of VEGF-A165 to VEGFR-2, as these two isoforms bind to VEGFR-2 with the same affinity as judged from Biocore analyses.[5] Dependent on its inability to engage NRP1 in the VEGFR-2 signaling complex and the loss of efficient phosphorylation at the positive regulatory sites, VEGF-A165b may therefore occupy VEGFR-2 without transducing a potent angiogenic effect. Another important question is why VEGF-A165b does not stimulate phosphorylation of the positive regulatory sites in VEGFR-2 as do the other VEGF-A isoforms tested? This may possibly be due to effects of VEGF-A165b on the rotation of the receptors in the dimer, making the Y1052/Y1057 less preferred substrates for the VEGFR-2 kinase or alternatively exposing these phosphosites to rapid dephosphorylation. It is possible that VEGF-A165b would induce differently rotated VEGFR-2 dimers in a manner directly or indirectly dependent on its unique COOH-terminal tail. That VEGF-A165b is folded differently than VEGF-A165 is conceivable as it does not bind to NRP1 and HS in spite of the fact that exon 7 is included in the primary sequence of both isoforms. Detailed structural analyses are required to prove the concept that VEGFR-2 dimers have different properties when induced by VEGF-A165b compared with VEGF-A165.

[5] A. Varey et al., unpublished data.

Disclosure of Potential Conflicts of Interest

S.J. Harper and D. Bates are coinventors on the patent describing VEGF-165b as a potential therapeutic. The other authors disclosed no potential conflicts of interest.

Acknowledgments

Received 12/10/2007; revised 3/29/2008; accepted 4/10/2008.

Grant support: Swedish Cancer Society (project no. 3820-B05-10XBC), Swedish Research Council (project K-2005-32X-12552-08A), and Novo Nordisk Foundation (L. Claesson-Welsh).

The costs of publication of this article were defrayed in part by the payment of page charges. This article must therefore be hereby marked *advertisement* in accordance with 18 U.S.C. Section 1734 solely to indicate this fact.

We thank Drs. Lars Jakobsson (Cancer UK, London, United Kingdom) and Emma Rennel (University of Bristol, Bristol, United Kingdom) for their contributions to this work and critical reading of the manuscript and Drs. Georg Breier, Lars Holmgren, Michael Klagsbrun, and Andras Nagy for their generosity in making their valuable reagents available to us.

References

1. Ferrara N. The role of VEGF in the regulation of physiological and pathological angiogenesis. EXS 2005;94:209–31.
2. Muller YA, Li B, Christinger HW, Wells JA, Cunningham BC, de Vos AM. Vascular endothelial growth factor: crystal structure and functional mapping of the kinase domain receptor binding site. Proc Natl Acad Sci U S A 1997;94:7192–7.
3. Shima DT, Kuroki M, Deutsch U, Ng YS, Adamis AP, D'Amore PA. The mouse gene for vascular endothelial growth factor. Genomic structure, definition of the transcriptional unit, and characterization of transcriptional and post-transcriptional regulatory sequences. J Biol Chem 1996;271:3877–83.
4. Bates DO, Cui TG, Doughty JM, et al. VEGF165b, an inhibitory splice variant of vascular endothelial growth factor, is down-regulated in renal cell carcinoma. Cancer Res 2002;62:4123–31.
5. Olsson AK, Dimberg A, Kreuger J, Claesson-Welsh L. VEGF receptor signalling—in control of vascular function. Nat Rev Mol Cell Biol 2006;7:359–71.
6. Ferrara N, Carver-Moore K, Chen H, et al. Heterozygous embryonic lethality induced by targeted inactivation of the VEGF gene. Nature 1996;380:439–42.
7. Carmeliet P, Ferreira V, Breier G, et al. Abnormal blood vessel development and lethality in embryos lacking a single VEGF allele. Nature 1996;380:435–9.
8. Shalaby F, Rossant J, Yamaguchi TP, et al. Failure of blood-island formation and vasculogenesis in Flk-1-deficient mice. Nature 1995;376:62–6.
9. Cross MJ, Dixelius J, Matsumoto T, Claesson-Welsh L. VEGF-receptor signal transduction. Trends Biochem Sci 2003;28:488–94.
10. Jia H, Bagherzadeh A, Hartzoulakis B, et al. Characterization of a bicyclic peptide neuropilin-1 (NP-1) antagonist (EG3287) reveals importance of vascular endothelial growth factor exon 8 for NP-1 binding and role of NP-1 in KDR signaling. J Biol Chem 2006;281:13493–502.
11. Esko JD, Selleck SB. Order out of chaos: assembly of ligand binding sites in heparan sulfate. Annu Rev Biochem 2002;71:435–71.
12. Dougher AM, Wasserstrom H, Torley L, et al. Identification of a heparin binding peptide on the extracellular domain of the KDR VEGF receptor. Growth Factors 1997;14:257–68.
13. Jakobsson L, Kreuger J, Holmborn K, et al. Heparan sulfate in *trans* potentiates VEGFR-mediated angiogenesis. Dev Cell 2006;10:625–34.
14. He Z, Tessier-Lavigne M. Neuropilin is a receptor for the axonal chemorepellent Semaphorin III. Cell 1997;90:739–51.
15. Kolodkin AL, Levengood DV, Rowe EG, Tai YT, Giger RJ, Ginty DD. Neuropilin is a semaphorin III receptor. Cell 1997;90:753–62.
16. Soker S, Takashima S, Miao HQ, Neufeld G, Klagsbrun M. Neuropilin-1 is expressed by endothelial and tumor cells as an isoform-specific receptor for vascular endothelial growth factor. Cell 1998;92:735–45.
17. Kawasaki T, Kitsukawa T, Bekku Y, et al. A requirement for neuropilin-1 in embryonic vessel formation. Development 1999;126:4895–902.
18. Cebe Suarez S, Pieren M, Cariolato L, et al. A VEGF-A splice variant defective for heparan sulfate and neuropilin-1 binding shows attenuated signaling through VEGFR-2. Cell Mol Life Sci 2006;63:2067–77.
19. Woolard J, Wang WY, Bevan HS, et al. VEGF165b, an inhibitory vascular endothelial growth factor splice variant: mechanism of action, *in vivo* effect on angiogenesis and endogenous protein expression. Cancer Res 2004;64:7822–35.
20. Varey AH, Rennel ES, Qiu Y, et al. VEGF(165)b, an antiangiogenic VEGF-A isoform, binds and inhibits bevacizumab treatment in experimental colorectal carcinoma: balance of pro- and antiangiogenic VEGF-A isoforms has implications for therapy. Br J Cancer 2008;98:1366–79.
21. Rennel ES, Waine E, Guan H, et al. The endogenous anti-angiogenic VEGF isoform, VEGF(165)b inhibits human tumour growth in mice. Br J Cancer 2008;98:1250–7.
22. Waltenberger J, Claesson-Welsh L, Siegbahn A, Shibuya M, Heldin CH. Different signal transduction properties of KDR and Flt1, two receptors for vascular endothelial growth factor. J Biol Chem 1994;269:26988–95.
23. Rennel ES, H-Zadeh MA, Wheatley E, et al. Recombinant human VEGF165b protein is an effective anticancer agent in mice. Eur J Cancer. In press 2008.
24. Matsumoto T, Bohman S, Dixelius J, et al. VEGF receptor-2 Y951 signaling and a role for the adapter molecule TSAd in tumor angiogenesis. EMBO J 2005;24:2342–53.
25. Li X, Edholm D, Lanner F, et al. Lentiviral rescue of VEGFR-2 expression in flk1−/− ES cells shows early priming of endothelial precursors. Stem Cells 2007;25:2987–95.
26. Jakobsson L, Kreuger J, Claesson-Welsh L. Building blood vessels—stem cell models in vascular biology. J Cell Biol 2007;177:751–5.
27. Dixelius J, Makinen T, Wirzenius M, et al. Ligand-induced vascular endothelial growth factor receptor-3 (VEGFR-3) heterodimerization with VEGFR-2 in primary lymphatic endothelial cells regulates tyrosine phosphorylation sites. J Biol Chem 2003;278:40973–9.
28. Landgren E, Schiller P, Cao Y, Claesson-Welsh L. Placenta growth factor stimulates MAP kinase and mitogenicity but not phospholipase C-γ and migration of endothelial cells expressing Flt 1. Oncogene 1998;16:359–67.
29. Kreuger J, Lindahl U, Jemth P. Nitrocellulose filter binding to assess binding of glycosaminoglycans to proteins. Methods Enzymol 2003;363:327–39.
30. Ito N, Wernstedt C, Engstrom U, Claesson-Welsh L. Identification of vascular endothelial growth factor receptor-1 tyrosine phosphorylation sites and binding of SH2 domain-containing molecules. J Biol Chem 1998;273:23410–8.
31. Poltorak Z, Cohen T, Sivan R, et al. VEGF145, a secreted vascular endothelial growth factor isoform that binds to extracellular matrix. J Biol Chem 1997;272:7151–8.

Vascular Endothelial Growth Factor (VEGF)-A165b Is a Weak *In vitro* Agonist for VEGF Receptor-2 Due to Lack of Coreceptor Binding and Deficient Regulation of Kinase Activity

Harukiyo Kawamura, Xiujuan Li, Steven J. Harper, et al.

Cancer Res 2008;68:4683-4692.